Planar nearfield acoustical holography in moving fluid medium at subsonic and uniform velocity[a)]

Hyu-Sang Kwon
Acoustics and Vibration Laboratory, Korea Research Institute of Standards and Science, P.O. Box 102, Yuseong, Deajon 305-340, South Korea

Yaying Niu and Yong-Joe Kim[b)]
Department of Mechanical Engineering, Acoustics and Signal Processing Laboratory, Texas A&M University, 3123 TAMU, College Station, Texas 77843-3123

(Received 25 January 2010; revised 12 July 2010; accepted 14 July 2010)

Nearfield acoustical holography (NAH) data measured by using a microphone array attached to a high-speed aircraft or ground vehicle include significant airflow effects. For the purpose of processing the measured NAH data, an improved nearfield acoustical holography procedure is introduced that includes the effects of a fluid medium moving at a subsonic and uniform velocity. The convective wave equation along with the convective Euler's equation is used to develop the proposed NAH procedure. A mapping function between static and moving fluid medium cases is derived from the convective wave equation. Then, a conventional wave number filter designed for static fluid media is modified to be applicable to the moving fluid cases by applying the mapping function to the static wave number filter. In order to validate the proposed NAH procedure, a monopole simulation at the airflow speed of Mach=−0.6 is conducted. The reconstructed acoustic fields obtained by applying the proposed NAH procedure to the simulation data agree well with directly-calculated acoustic fields. Through an experiment with two loudspeakers performed in a wind tunnel operating at Mach=−0.12, it is shown that the proposed NAH procedure can be also used to reconstruct the sound fields radiated from the two loudspeakers. © *2010 Acoustical Society of America.* [DOI: 10.1121/1.3478771]

PACS number(s): 43.60.Sx, 43.28.Py, 43.35.Sx [EGW] Pages: 1823–1832

I. INTRODUCTION

Nearfield Acoustical Holography (NAH) is a powerful tool that can be used to visualize three-dimensional sound fields by projecting acoustic pressure data measured on a two-dimensional (2-D) measurement surface (i.e., hologram surface) to reconstruction surfaces. The NAH procedure that includes evanescent wave components (i.e., subsonic wave components) to improve the spatial resolution of a reconstructed sound field was first introduced by Williams *et al.* in 1980s.[1–3] Since then, many researchers have improved the NAH procedure and applied the improved NAH procedures to various vibro-acoustic and aeroacoustic problems.

When the acoustic pressure data measured on a hologram surface are projected by using a NAH procedure, the acoustic pressure data are required to be "spatially coherent": i.e., an acoustic pressure signal measured at a microphone location should be coherent to an acoustic pressure signal measured at another measurement location. That is, it is required that there is only a single coherent source in the system of interest, or that all measurement points in a measurement aperture are measured simultaneously. The former condition is not always satisfied since a "real" system usually has a composite source consisting of multiple incoherent sources: e.g., the noise source of an electric fan can consist of multiple incoherent sources, each associated with electric motor noise, blade vibration noise, flow noise induced by vortex-shedding at the edges of blades, and so on. The latter condition requires a large number of microphones that completely cover a composite source although extensive research has been conducted to project the acoustic pressure data measured only on a small patch of a complete measurement aperture.[4–8]

In order to satisfy the coherence requirement, a scan-based, multi-reference NAH procedure was introduced by Hald.[9] In this procedure, a small number of microphones can be used to measure acoustic pressure data on a patch of a complete hologram surface during each scanning measurement, while multiple reference microphones are fixed at their locations throughout the scanning measurements. The measured patch data are combined to obtain a complete data set on the entire hologram surface. The combined hologram data are then decomposed into partial acoustic pressure fields, each is spatially coherent. Note that the partial field decomposition procedure based on the Singular Value Decomposition (SVD) was first introduced by Hald.[9] Each partial acoustic pressure field on the hologram surface is repetitively projected onto reconstruction surfaces and the total projected fields are then calculated by superposing all of the projected partial fields.

[a)]Portions of this work are presented in "Planar nearfield acoustical holography in high-speed, subsonic flow," in Proceedings of Noise-Con 2010 Conference, Baltimore, April 2010.

[b)]Author to whom correspondence should be addressed. Electronic mail: joekim@tamu.edu

Note that the scan-based, multi-reference NAH procedure is based on an assumption that the sound field radiated from a composite source is stationary during scanning measurements: i.e., there should be no temporal variation of the radiated sound field in a statistical sense. However, in a "real" NAH measurement, the sound field is not always stationary resulting in non-stationarity effects. For the purpose of reducing the non-stationarity effects, a source non-stationarity compensation procedure was introduced by Kwon *et al.*, provided that source levels are assumed to be non-stationary while their directivities remain statistically unchanged during entire scanning measurements.[10]

In order to obtain "physically-meaningful" partial fields from a scan-based, multi-reference NAH measurement, it is required to place reference microphones close to noise sources.[11] Then, each of the resulting partial fields can be associated with a specific noise source whose noise signal is closely correlated with the signal measured by a reference microphone. However, it is not always possible to physically place reference microphones close to noise sources. Kim *et al.* proposed to use virtual references of which locations are determined where beamforming powers are maximized, which allows to identify physically-meaningful partial fields regardless of the physical locations of the reference microphones.[11]

When a NAH measurement is performed using a microphone array fixed on a moving transportation means such as a moving airplane or ground vehicle, the measured data includes the effects of a moving fluid medium. For example, jet noise data can be measured by using an array of pressure transducers mounted on the fuselage surface of an aircraft during its cruise condition, e.g., at $M=0.5-0.8$ where M represents the Mach number. The measured data can be then used to visualize jet noise pattern radiated from jet engine to the fuselage surface.

In the aforementioned jet noise measurement case, it can be assumed that Turbulence Boundary Layer (TBL) noise can be negligible in the measured data. Consider the cross-spectral matrix of microphone array signals whose (m,n) element is the cross-spectrum between the m- and n-th microphone signals. The off-diagonal terms of the cross-spectral matrix associated with the TBL noise can be reduced when the distance of any two adjacent microphones is larger than TBL correlation length. In order to reduce the diagonal terms of the cross-spectral matrix (i.e., auto-spectra), microphone fairings can be used to generate smooth streamlines around the microphones. These smooth streamlines then result in low auto-spectral, flow noise levels.

Another example can be the tire noise data measured by using a microphone array attached to a moving ground vehicle. Note that the latter measurement case can be equivalent to a case where a composite source and receiver are not in motion while a fluid medium is moving at a uniform velocity.

Ruhala *et al.* proposed a planar NAH procedure in a fluid medium moving at a low subsonic speed.[12] In this low-speed case, a static radiation circle in the (k_x,k_y) wave number domain is assumed to shift along the wave number axis in the opposite flow direction while its radius increases due to the motion of the fluid medium. Thus, they proposed the NAH procedure that uses a modified wave number filter based on the shifted and extended radiation circle. However, when the fluid medium is moving at a high Mach number (e.g., $0.2<|M|<1$), the shifted and extended radiation circle that is represented in Eq. (42) of Ref. 12 is no longer valid. It is also assumed that the particle velocities perpendicular to the flow direction are not affected by the mean flow as described right below Eq. (44) in Ref. 12, which is not valid for a moving fluid medium at a high Mach number. Thus, the low-speed approximations used in the NAH procedure proposed by Ruhala *et al.* result in significant errors when the fluid medium is moving at a high Mach number.

In the present paper, an improved NAH procedure is developed that is applicable to high-speed, subsonic flow conditions. In particular, a mapping function between static and moving medium cases is derived from the convective wave equation. A wave number filter that can be applied to both high- and low-speed, subsonic flow cases is then defined by mapping the conventional static wave number filter[3,13] to the coordinate system of a moving fluid medium case. Here, it is also proposed to consider the flow effects on reconstructed particle velocities in the flow direction as well as in the directions perpendicular to the flow direction. Note that the proposed NAH procedure can be applied to any subsonic, uniform flow conditions where $|M|<1$. For the purpose of validating the proposed NAH procedure, a monopole simulation at the airflow speed of $M=-0.6$ is conducted. The negative Mach number indicates that the fluid flow direction is opposite to a predefined positive coordinate direction. This high Mach number is chosen to simulate a jet noise measurement case where a jet airplane is in a cruise condition at $|M|=0.6$ as described before. An experiment with two loudspeakers in a wind tunnel operating at $M=-0.12$ is also conducted.

In this paper, it is assumed that the flow noise induced by placing array microphones in a high-speed, moving fluid medium can be ignored. A cross-spectral matrix between reference microphone signals is measured by placing reference microphones at the locations where the effects of flow are negligible but the source signals are measurable. Then, the cross-spectral matrix is decomposed by applying the Singular Value Decomposition (SVD). The microphone-induced flow noise components can be then reduced from the measured data by removing the singular values associated with the flow noise components. The experimental results presented in this article are processed by using the aforementioned flow-induced noise reduction procedure.

In the following theory sections, spatially-coherent, partial acoustic pressure fields on a hologram surface are assumed to be given. For the numerical and experimental results presented in this article, the spatially-coherent, partial acoustic pressure fields are obtained by applying the non-stationarity compensation and partial field decomposition procedures[10,11] to the calculated or measured acoustic pressure data on the hologram surface.

II. THEORY

A. Planar NAH in static fluid medium

In order to present the proposed NAH procedure in a consistent and comprehensive manner, consider a conventional NAH procedure that can be applied to a static case where noise sources, receiver, and fluid medium are not in motion. A Cartesian coordinate system in the static case is defined as (x,y,z). When acoustic pressure is measured on a measurement plane at $z=z_h$ (i.e., hologram plane), the measured acoustic pressure data can be decomposed into spatially-coherent, partial acoustic pressure fields: i.e., each resulting partial field is uncorrelated with other partial fields.[9–11] Each partial acoustic pressure field, $p(x,y,z_h,\omega)$ can be then expressed as a superposition of plane wave components by applying the spatial Fourier Transform in the x- and y-directions. The resulting plane wave component, $P(k_x,k_y,z_h,\omega)$ (i.e., acoustic pressure spectrum) in the wave number domain, (k_x,k_y), can be written as

$$P(k_x,k_y,z_h,\omega)=\mathbf{F}[p(x,y,z_h,\omega)], \tag{1}$$

where $\mathbf{F}$ represents the 2-D spatial Fourier Transform. Note that in a real implementation, the spatial Fast Fourier Transform (FFT) is applied to the spatially-sampled, acoustic pressure data instead of the spatial Fourier Transform.

The acoustic pressure spectrum on a reconstruction surface at $z=z_r$ can be calculated from the measured acoustic pressure spectrum on the hologram surface by multiplying a plane wave propagator: i.e.,

$$P(k_x,k_y,z_r,\omega)=P(k_x,k_y,z_h,\omega)K_p(k_x,k_y,z_r-z_h,\omega). \tag{2}$$

In Eq. (2), K_p is the acoustic pressure propagator defined as

$$K_p(k_x,k_y,z,\omega)=\exp(ik_z z), \tag{3}$$

where

$$k_z=\begin{cases}\sqrt{k^2-k_x^2-k_y^2} & \text{if } k_x^2+k_y^2\le k^2\\ i\sqrt{k_x^2+k_y^2-k^2} & \text{otherwise.}\end{cases} \tag{4}$$

In Eq. (4), k is the wave number defined as $k=\omega/c_0$ where c_0 is the speed of sound. The projected particle velocity spectrum can be also obtained by applying the Euler's equation to Eq. (2). The particle velocity propagator is then defined as

$$K_j(k_x,k_y,z,\omega)=\frac{k_j}{\rho_0 c_0 k}\exp(ik_z z)(j=x,y,\text{or } z), \tag{5}$$

where ρ_0 is the static density of the fluid medium. Thus, the projected particle velocity spectrum in the j-direction can be obtained from Eq. (2) by replacing K_p with K_j.

The circle with the radius of $r=k$ obtained by setting $k_z=0$ in Eq. (4) is referred to as the radiation circle[3,14]; i.e.,

$$\frac{k_x^2}{k^2}+\frac{k_y^2}{k^2}=1. \tag{6}$$

Note that the propagator of the evanescent wave component outside of the radiation circle that is applied during a backward NAH projection improves the spatial resolution of a reconstructed sound field.[1–3] However, measurement noise outside of the radiation circle is also amplified exponentially during the backward projection procedure. For the purpose of suppressing the noise effects, it is recommended to apply a static wave number filter[3,13] to the acoustic pressure spectrum before performing the backward NAH projection.

The reconstructed acoustic pressure or particle velocity field is obtained by applying the inverse spatial Fourier Transform to the projected acoustic pressure or particle velocity spectrum: e.g.,

$$p(x,y,z_r,\omega)=\mathbf{F}^{-1}[P(k_x,k_y,z_r,\omega)]. \tag{7}$$

The aforementioned NAH procedure is repetitively applied to all of the partial fields on the hologram surface. The projected fields are then combined to obtain a total field on the reconstruction surface.[10,11] The projected sound intensity field can be also calculated by multiplying the projected acoustic pressure and particle velocity fields.

B. Plane wave propagation in moving fluid medium

Consider a coordinate system, (χ,ψ,ζ) in a moving medium that is corresponding to the (x,y,z) coordinate system in the static fluid medium. When the fluid medium is moving at a subsonic and uniform χ-direction velocity, U while a composite noise source and receiver are not in motion, the convective wave equation[14] can be written as

$$\nabla^2 p=\frac{1}{c_0^2}\frac{D^2 p}{Dt^2}, \tag{8}$$

where D/Dt is the total derivative (or the material derivative) defined as

$$\frac{D}{Dt}=\frac{\partial}{\partial t}+U\frac{\partial}{\partial \chi}. \tag{9}$$

The convective Euler's equation[14] that relates acoustic pressure and particle velocity can be also written in terms of the total derivative: i.e.,

$$\rho_0\frac{D\vec{v}}{Dt}=-\vec{\nabla}p. \tag{10}$$

For the purpose of analyzing the plane wave propagation characteristics in the moving fluid medium, consider the following plane wave solutions for the acoustic pressure and particle velocity represented as

$$p(\chi,\psi,\zeta,t)=P\exp[i(k_\chi\chi+k_\psi\psi+k_\zeta\zeta-\omega t)], \tag{11}$$

and

$$v_j(\chi,\psi,\zeta,t)=V_j\exp[i(k_\chi\chi+k_\psi\psi+k_\zeta\zeta-\omega t)], \tag{12}$$

where the subscript, j represents the particle velocity direction (i.e., $j=\chi$, ψ, or ζ). By applying the acoustic pressure solution, Eq. (11) into Eq. (8), the characteristic equation can be found as

$$k_\zeta^2=k^2-(1-M^2)k_\chi^2-2kMk_\chi-k_\psi^2. \tag{13}$$

In Eq. (13), M is the Mach number defined as

$$M = \frac{U}{c_0}. \tag{14}$$

Similarly, by substituting Eqs. (11) and (12) into Eq. (10), the acoustic pressure and particle velocity can be related as

$$V_j = \frac{k_j}{\rho_0 c_0 (k - Mk_\chi)} P. \tag{15}$$

By setting $k_\zeta = 0$ in Eq. (13), an ellipse can be obtained that defines the borderline between supersonic and subsonic components: i.e.,

$$\frac{(k_\chi + a)^2}{r_1^2} + \frac{k_\psi^2}{r_2^2} = 1, \tag{16}$$

where

$$a = \frac{kM}{1 - M^2}, \tag{17}$$

$$r_1 = \frac{k}{1 - M^2}, \tag{18}$$

and

$$r_2 = \frac{k}{\sqrt{1 - M^2}}. \tag{19}$$

Equation (16) represents the ellipse with the semimajor axis, r_1 and semiminor axis, r_2 centered at $(-a, 0)$. This ellipse can be defined as the "radiation ellipse" that is corresponding to the radiation circle in the case of the static fluid medium: i.e., the wave components inside of the radiation ellipse represent propagating waves while the outside wave components represent evanescent waves.

When compared with the radiation circle in Eq. (6), the center of the radiation ellipse shifts by $-a$ along the k_χ-axis in the flow direction (i.e., the χ-direction). The radius, $r=k$ of the static radiation circle increases to r_1 in the k_χ-direction and r_2 in the k_ψ-direction in the case of the subsonic flow (i.e., $|M|<1$). Although there is no flow in the ψ-direction, the semiminor axis, r_2 is larger than the radius of the static radiation circle, $r=k$: thus, the flow effects in the directions perpendicular to the flow direction cannot be ignored at a high Mach number. From Eqs. (6) and (16), a mapping function that maps the radiation circle in the (k_x, k_y) domain into the radiation ellipse in the (k_χ, k_ψ) domain is defined as

$$(k_x, k_y) = (k(k_\chi + a)/r_1, kk_\psi/r_2). \tag{20}$$

The mapping of the radiation circle to radiation ellipse is illustrated in Fig. 1.

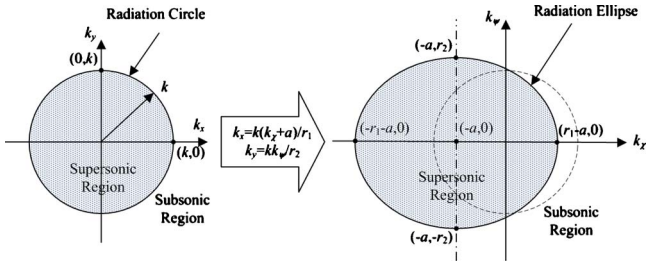

FIG. 1. (Color online) Mapping of radiation circle ($M=0$) to radiation ellipse ($0<|M|<1$).

C. NAH procedure in moving fluid medium

When acoustic pressure data are measured in a moving fluid medium, the forward and inverse spatial Fourier Transforms given in Eqs. (1) and (7) can be re-used without any modifications. Note that the Fourier Transforms in the moving fluid medium case relate the acoustic fields between (χ, ψ) and (k_χ, k_ψ) domains. From Eqs. (3), (5), (13), and (15), the acoustic pressure and particle velocity propagators are defined as

$$K_p(k_\chi, k_\psi, \zeta, \omega) = \exp(ik_\zeta \zeta), \tag{21}$$

and

$$K_j(k_\chi, k_\psi, \zeta, \omega) = \frac{k_j}{\rho_0 c_0 (k - Mk_\chi)} \exp(ik_\zeta \zeta) \quad (j = \chi, \psi, \text{or } \zeta), \tag{22}$$

where

$$k_\zeta = \begin{cases} \sqrt{k^2 - (1 - M^2)k_\chi^2 - 2kMk_\chi - k_\psi^2} & \text{if } (1 - M^2)k_\chi^2 + 2kMk_\chi + k_\psi^2 \le k^2 \\ i\sqrt{(1 - M^2)k_\chi^2 + 2kMk_\chi + k_\psi^2 - k^2} & \text{otherwise.} \end{cases} \tag{23}$$

An improved wave number filter is obtained by mapping the conventional static wave number filter[3,13] in the (k_x, k_y) domain into the (k_χ, k_ψ) domain. By applying Eq. (20) to Eqs. (A1)–(A3) in Appendix A, the wave number filter in the moving fluid medium case is defined as:

If $k_c \ge k$,

$$W(k_\chi, k_\psi) = \begin{cases} 1 - \exp[(k_r/k_c - 1)/\alpha]/2 & \text{if } k_r \le k_c \\ \exp[(k_r/k_c - 1)/\alpha]/2 & \text{otherwise.} \end{cases} \tag{24}$$

Otherwise,

$$W(k_\chi, k_\psi) = \begin{cases} 1 & \text{if } k_r \le k \\ 0 & \text{otherwise.} \end{cases} \tag{25}$$

In Eqs. (24) and (25), k_r is defined as

$$k_r = k\sqrt{(k_\chi + a)^2/r_1^2 + k_\psi^2/r_2^2}. \tag{26}$$

Note that k_r in Eqs. (24)–(26) is represented in terms of the moving medium coordinates, χ and ψ that is obtained by applying the mapping function, Eq. (20) to Eq. (A3). In Eq.

(24), α and k_c are the filter slope and cut-off wave number, respectively, that are determined from the dynamic range of a measurement system, signal-to-noise ratio (SNR), hologram height, and wave number components of a source (see Ref. 3).

D. Spatial sampling in moving fluid medium

As discussed in previous sections, the mean flow of a fluid medium affects the wave number spectrum in the flow direction as well as in the directions perpendicular to the flow direction. Thus, it is required to define the χ- and ψ-direction sampling spaces of a NAH microphone array placed in the moving fluid medium. In a static fluid medium case, the number of spatial sampling points along the minimum wavelength at the highest frequency of interest should be at least two: i.e., the sampling space, Δ is defined as

$$\Delta = \frac{\lambda_{\min}}{2s} = \frac{\pi}{sk_{\max}} = \frac{c_0}{2sf_{\max}}, \tag{27}$$

where s is the over-sampling rate ($s \geq 1$): e.g., it is recommended to set $s=2$ (i.e., four sampling points per unit wavelength). In Eq. (27), $\lambda_{\min}$ is the minimum wavelength that can be related with the maximum wave number, $k_{\max}$ or the maximum frequency, $f_{\max}$: i.e., $\lambda_{\min}=2\pi/k_{\max}=c_0/f_{\max}$. Note that $k_{\max}$ can be also considered as the radius of the radiation circle at the maximum frequency, $f_{\max}$. Similarly, the spatial sampling spaces in the case of the moving fluid medium can be determined from the radiation ellipse defined in Eqs. (16)–(19). The maximum wave numbers in the χ- and ψ-directions can be obtain from Eqs. (16)–(19): i.e.,

$$k_{\chi,\max} = \begin{cases} 2\pi f_{\max}/\{c_0(1-M)\} & \text{if } 0 \leq M < 1 \\ 2\pi f_{\max}/\{c_0(1+M)\} & \text{if } -1 < M < 0, \end{cases} \tag{28}$$

and

$$k_{\psi,\max} = \frac{2\pi f_{\max}}{c_0\sqrt{1-M^2}}. \tag{29}$$

By substituting the maximum wave numbers into Eq. (27), the spatial sampling spaces in the moving fluid medium are written as

$$\Delta_\chi = \begin{cases} c_0(1-M)/(2sf_{\max}) & \text{if } 0 \leq M < 1 \\ c_0(1+M)/(2sf_{\max}) & \text{if } -1 < M < 0, \end{cases} \tag{30}$$

and

$$\Delta_\psi = \frac{c_0\sqrt{1-M^2}}{2sf_{\max}}. \tag{31}$$

III. MONOPOLE SIMULATION AND EXPERIMENT

For the purpose of validating the proposed NAH procedure in a moving fluid medium, a monopole simulation and an experiment described in the following sections are conducted.

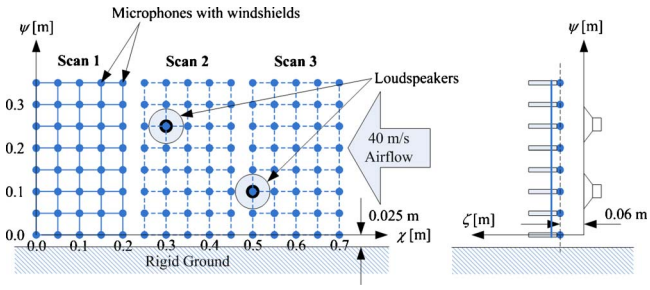

FIG. 2. (Color online) Sketch of experimental setup.

A. Monopole simulation

The mathematical representation of the acoustic pressure field radiated from a monopole in a moving fluid medium is presented as Eq. (B7) in Appendix B. Equation (B7) is implemented in a computer program and used for the simulation. Note that the speed of sound is set to $c_0=343$ m/s for the simulation.

The monopole simulation is designed to simulate the experiment shown in Figs. 2 and 3. An 8×5 microphone array is assumed to be used in the simulation. Note that the χ-direction microphone space is set to $d\chi=0.025$ m for the simulation while $d\chi=0.05$ m for the experiment. The ψ-direction microphone space and hologram height (i.e., the distance between the source and hologram surfaces) are set to $d\psi=0.05$ m and $\zeta_h=0.06$ m, respectively. The total number of scans is 6 in the simulation, which covers 8×30 measurement points.

In the simulation, two uncorrelated monopole sources are placed at the center locations of two loudspeakers used in the experiment, i.e., $(\chi,\psi,\zeta)=(0.3,0.25,-0.05)$ m and $(0.5,0.1,-0.05)$ m. It is assumed that there is no reflective surface (i.e., free field). Airflow speed is set to $M=-0.6$ that is chosen to simulate a jet noise measurement case where a jet airplane is in a cruise condition at $|M|=0.6$.

Acoustic pressure data are calculated at the locations of the array microphones at each scanning position for 10 s at the sampling frequency of 8192 Hz. The reference signals are also calculated at the locations of two reference microphones placed closely to the loudspeakers. Note that the distance between each monopole and reference microphone is 0.01 m.

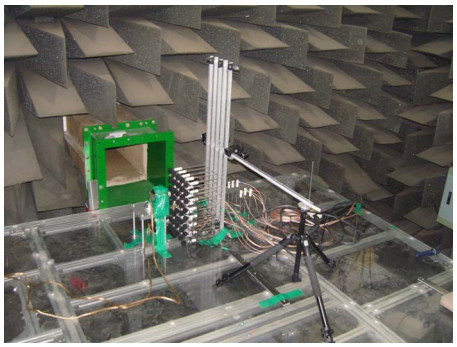

FIG. 3. (Color online) Photo of experimental setup: wind tunnel outlet, ground condition, microphone array, and two loudspeakers.

FIG. 4. (Color online) Photo of experimental setup: two HP signal generators, two-channel loudspeaker amplifier (in black), NI data acquisition system, and laptop.

B. Experiment setup

The experimental setup is shown in Figs. 2–4. An 8×5 quarter inch microphone array (i.e., the microphone's diameter is approximately 7 mm) is used to scan 8×15 measurement points: i.e., the total number of scans is 3 as shown in Fig. 2. The χ- and ψ-direction microphone spaces are 0.05 m and the hologram height is $\zeta_h = 0.06$ m. At each scanning position, acoustic pressure signals are recorded for 20 s at the sampling frequency of 8192 Hz. In order to reduce microphone-induced flow noise effects, a wind screen (shown as the spherical, black foam in Fig. 3) with a diameter of 0.03 m is installed at the tip of each array microphone.

Two loudspeakers are placed at $(\chi, \psi, \zeta) = (0.3, 0.25, 0)$ m and $(0.5, 0.1, 0)$ m where the χ- and ψ-coordinates represent the center locations of the loudspeakers. Note that the origin of the ζ-coordinate is set at the most front of the loudspeakers as shown in Fig. 2.

As shown in Figs. 2 and 3, there is a hard surface that can be assumed as a rigid boundary. The rigid surface is set at $\psi = 0$ so that the distance between the rigid surface and microphone array is one half of the ψ-direction microphone space (i.e., 0.025 m as shown in Fig. 2). The measured acoustic pressure data is then mirrored with respect to the rigid surface. The hologram data obtained by assembling both the measured and mirrored acoustic pressure data are then processed with the assumption that the combined hologram data are measured in a free-field condition.

An acoustic wind tunnel with an open test section of 0.4 m $\times$ 0.4 m is used to generate airflow at $M = -0.12$ in the experiment. Both the microphone array and loudspeakers are placed within the test section. The airflow speeds measured at several points within the test section verify that the airflow can be approximated as a uniform flow at the given flow condition of $M = -0.12$. In addition, it is measured that turbulence intensity is less than 1%. Background noise level is approximately 60 dBA within the test section.

A laptop along with a National Instrument (NI) 64 channel data acquisition (DAQ) system and the NI LabView software is used to record the acoustic pressure data as shown in Fig. 4. Two independent excitation signals are generated from two HP waveform generators. As shown in Fig. 4, the two waveform generators are placed on a black, two-channel loudspeaker amplifier and the NI DAQ system is placed behind the laptop. The excitation signals are then used to independently drive the loudspeakers through the two-channel amplifier. The maximum sound pressure levels (SPLs) are set to approximately 98 and 86 dB on the hologram plane at 1.5 kHz. Note that the higher SPL is set with the upper left loudspeaker and the lower SPL with the lower right loudspeaker. The excitation signals supplied to the amplifier are also used as reference signals. Additional reference signals are measured by using six reference microphones without wind screens installed. As shown in Fig. 3, the six reference microphones are placed behind the microphone array on the opposite side of the loudspeakers where flow noise effects can be negligible.

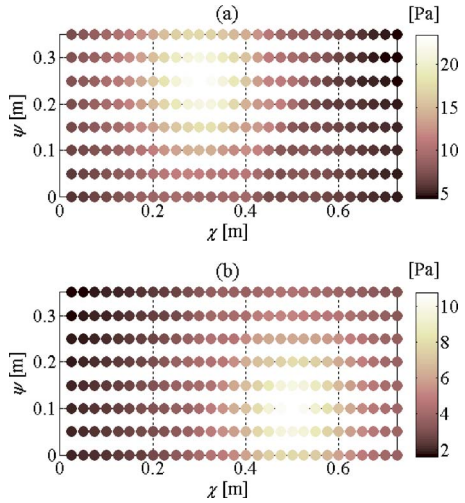

FIG. 5. (Color online) Acoustic pressure fields on hologram surface (monopole simulation results at $M = -0.6$ and $f = 1.5$ kHz): (a) First acoustic pressure field and (b) Second acoustic pressure field.

In order to reduce noise effects, the cross-spectral matrix of the reference signals is decomposed by applying the Singular Value Decomposition (SVD). The effects of flow noise and measurement noise are then reduced from the measured data by removing the third and higher largest singular values associated with the noise components. Note that the largest two singular values are mainly associated with the sound radiated from the loudspeakers.

C. Results and discussion

Note that the partial field decomposition procedure based on the Cholesky Decomposition (CD)[10,11] is applied to obtain the following partial field results. The acoustic pressure data generated from the two monopoles in an air medium moving at $M = -0.6$ are calculated on the hologram surface at $\zeta = 0.06$ m. The resulting hologram data are shown at $f = 1.5$ kHz in Fig. 5. Note that the first field is mainly radiated from the upper left monopole source and the second field from the lower right monopole source. The maximum SPL of the upper left monopole source is twice higher than the maximum SPL of the lower right one, which simulates the sound level difference between the two loudspeakers in the experiment.

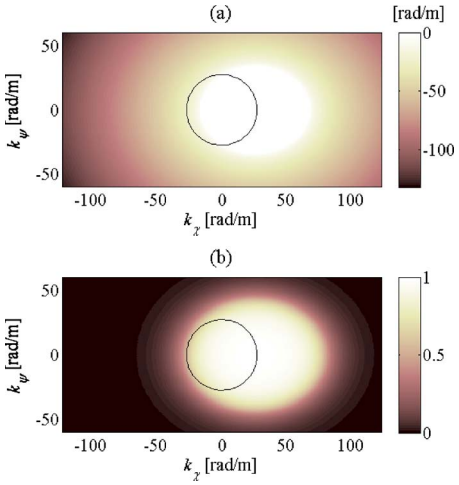

FIG. 6. (Color online) Two quantities in wave number domain when $M=-0.6$ and $f=1.5$ kHz (the black, solid-lined circle represents the static radiation circle when $c_0=343$ m/s): (a) Imaginary part of wave number, k_ζ [see Eq. (23)] and (b) weighting function, W of proposed wave number filter [see Eqs. (23)–(26)].

Figure 6 shows the imaginary part of the ζ-direction wave number, k_ζ and the weight function, W of the proposed wave number filter used for a backward projection as the functions of k_χ and k_ψ [see Eqs. (23)–(26)]. The radiation circle of the corresponding static fluid medium case (i.e., the no flow case at $f=1.5$ kHz) is overlaid as the black, solid-lined circle in Fig. 6. In Fig. 6(a), a radiation ellipse can be identified along the edge of the supersonic region where the imaginary part of k_ζ is equal to zero. Note that the center of the radiation ellipse is shifted along the positive k_χ-axis due to the negative fluid flow, i.e., at $M=-0.6$ [see Eqs. (16) and (17)]. In Fig. 6(b), the proposed wave number filter used for a backward projection, passes supersonic components (i.e., $W\cong 1$) while it reduces the most of high wave number, subsonic components with a smooth transition around the edge of the radiation ellipse.

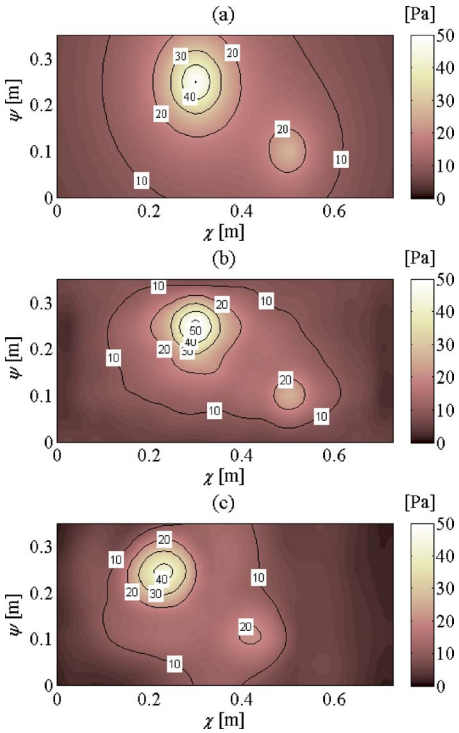

FIG. 7. (Color online) Total acoustic pressure fields on source plane at $\zeta=0$ m (monopole simulation results at $M=-0.6$ and $f=1.5$ kHz): (a) Directly calculated, (b) reconstructed by using "proposed" wave number filter, and (c) reconstructed by using conventional "static" wave number filter.

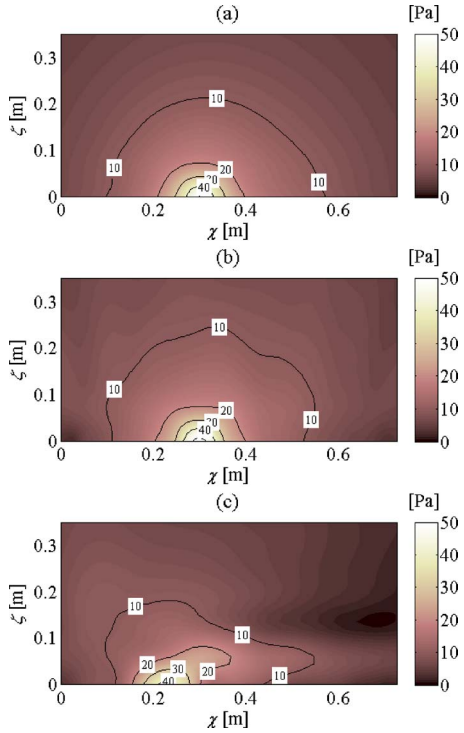

FIG. 8. (Color online) Total acoustic pressure fields on ζ-χ plane at $\psi=0.25$ m (monopole simulation results at $M=-0.6$ and $f=1.5$ kHz): (a) Directly calculated, (b) reconstructed by using "proposed" wave number filter, and (c) reconstructed by using conventional "static" wave number filter.

Figure 7 shows the directly-calculated and reconstructed total acoustic pressure fields on the source surface (i.e., $\zeta=0$ m) at $f=1.5$ kHz. The directly-calculated acoustic pressure field is shown in Fig. 7(a), while the reconstructed acoustic pressure fields are presented in Figs. 7(b) and 7(c). Note that the acoustic pressure field reconstructed by using the "proposed" wave number filter is shown in Fig. 7(b) while the acoustic pressure field reconstructed by using the conventional "static" wave number filter is shown in Fig. 7(c). The same results are also presented on the ζ-χ plane at $\psi=0.25$ m in Fig. 8. The reconstructed field by using the proposed wave number filter agrees well with the directly-calculated field except the edges of the measurement aperture: see the 10 Pa contour lines in Figs. 7(a) and 7(b). Note that the proposed NAH projection requires that the measured acoustic pressure along the edges of the measurement aperture should be negligibly small to reduce truncation errors. However, as shown in Fig. 5, the hologram acoustic pressure at the top and bottom edges close to sound sources cannot be negligible, resulting in the differences along the edges of the measurement aperture between the directly-calculated and reconstructed acoustic pressure fields in Figs. 7(a) and 7(b). When the directly-calculated field is compared with the acoustic pressure field reconstructed by using the conven-

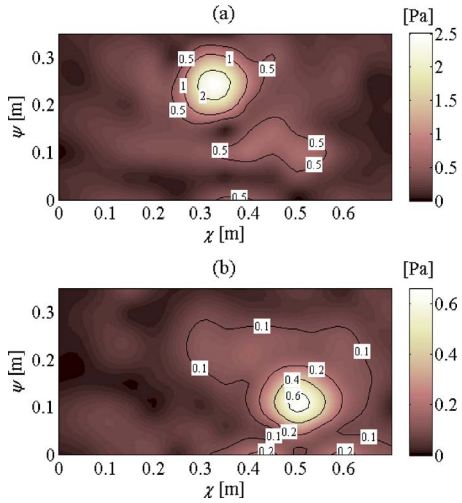

FIG. 9. (Color online) Reconstructed acoustic pressure fields on the source surface at $\zeta=0$ m (experimental results at $M=-0.12$ and $f=1.5$ kHz): (a) First acoustic pressure field, and (b) second acoustic pressure field.

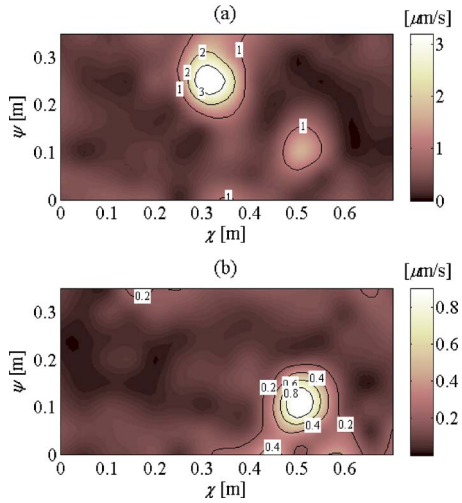

FIG. 10. (Color online) Reconstructed ζ-direction particle velocity fields in μm/s on source surface at $\zeta=0$ m (experimental results at $M=-0.12$ and $f=1.5$ kHz): (a) First ζ-direction particle velocity field, and (b) second ζ-direction particle velocity field.

tional "static" wave number filter, the locations of the sources identified from the reconstructed field are approximated 0.08 m shifted from the exact locations in the negative χ-direction [see Figs. 7(a) and 7(c)].

Figure 9 shows the acoustic pressure fields on the source surface at $\zeta=0$ m reconstructed from the experimental data at 1.5 kHz and the airflow speed of $M=-0.12$. Each acoustic pressure field represents the acoustic pressure field radiated from one of the loudspeakers. That is, the first acoustic pressure field is mainly associated with the sound radiated from the upper left loudspeaker and the second field from the lower right loudspeaker, although the small power leakage radiated from the lower right loudspeaker can be observed in the first field at the location of the lower right loudspeaker [see the 0.5 Pa contour line in Fig. 9(a)]. The two local maximum points of the projected acoustic pressure results in Fig. 9 are also in line with the locations of the two loudspeakers. Note that the maximum SPL of the first acoustic pressure field is approximately four time higher than the maximum SPL of the second field (i.e., 12 dB difference), which is consistent with the 12 dB difference between the loudspeaker excitation levels as described in Sec. III B.

The reconstructed ζ-direction particle velocity fields and active intensity fields on the source surface are presented in Figs. 10 and 11, respectively. Note that the reconstructed velocity and intensity are plotted in μm/s and μN/ms, respectively. Similar to the reconstructed acoustic pressure fields, the two loudspeaker locations can be identified from the reconstructed velocity and intensity results. The power leakage that has the circular shape of the lower right loudspeaker can be obviously observed in the first fields of Figs. 10 and 11 [see the 1 μm/s contour line in Fig. 10(a) and the 0.1 μN/ms contour line in Fig. 11(a)]. Note that in Fig. 9, the leakage is difficult to be associated with the lower right loudspeaker since its shape is not circular [see the 0.5 Pa contour line in Fig. 9(a)]. Through the reconstructed acoustic fields presented in Figs. 7 and 8, it can be concluded that although there is the power leakage, the CD-based partial field decomposition procedure results in the physically-meaningful partial fields.

IV. CONCLUSIONS

In this paper, the improved NAH procedure is presented that can be used to project acoustic pressure data measured in a fluid medium moving at a subsonic and uniform velocity while a composite noise source and receiver are not in motion. In particular, the wave number filter defined by mapping the static wave number filter into the wave number domain of the moving fluid medium is proposed. The particle velocity propagators are also introduced that include the mean flow effects on reconstructed particle velocities even in the directions perpendicular to the flow direction. By applying the proposed NAH procedure to the monopole simulation data at the airflow speed of $M=-0.6$, it is shown that the

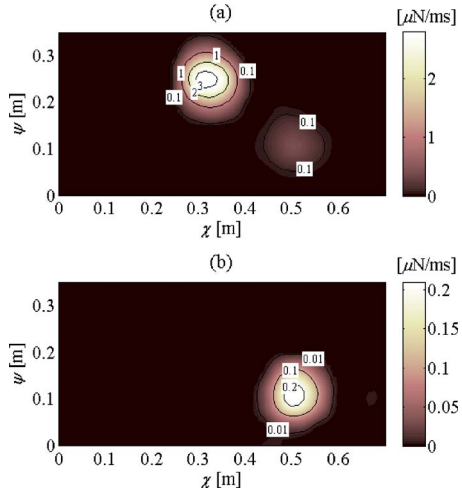

FIG. 11. (Color online) Reconstructed ζ-direction active intensity fields in μN/ms on source surface at $\zeta=0$ m (experimental results at $M=-0.12$ and $f=1.5$ kHz): (a) First ζ-direction active intensity field, and (b) second ζ-direction active intensity field.

proposed procedure can be used to successfully reproduce the directly-calculated sound fields. Through the experiment conducted with the two loudspeakers in the wind tunnel operating at $M=-0.12$, it is also shown that the proposed NAH procedure can be successfully used to identify the locations of the two loudspeakers and their radiation patterns.

APPENDIX A: WAVE NUMBER FILTER IN STATIC FLUID MEDIUM

The static wave number filter[3,13] is presented below: If $k_c \geq k$,

$$W(k_x,k_y)=\begin{cases}1-\exp[(k_r/k_c-1)/\alpha]/2 & \text{if } k_r \leq k_c \\ \exp[(1-k_r/k_c)/\alpha]/2 & \text{otherwise.}\end{cases} \tag{A1}$$

Otherwise,

$$W(k_x,k_y)=\begin{cases}1 & \text{if } k_r \leq k \\ 0 & \text{otherwise.}\end{cases} \tag{A2}$$

In Eqs. (A1) and (A2), k_r is defined as

$$k_r=\sqrt{k_x^2+k_y^2}. \tag{A3}$$

In Eq. (A1), α and k_c are the filter slope and cut-off wave number, respectively, that are determined from the dynamic range of a measurement system, signal-to-noise ratio (SNR), hologram height, z_h, and the wave number components of a source (see Ref. 3).

APPENDIX B: MONOPOLE IN MOVING FLUID MEDIUM

The acoustic pressure field radiated from a monopole in a moving fluid medium is introduced in this Appendix. It is assumed that the flow velocity of the fluid medium is subsonic and uniform in the x-direction while the monopole and receiver are fixed in a space. Since it is difficult to solve a non-homogeneous convective wave equation, it is here proposed to consider the case of a static fluid medium (i.e., the fluid medium is not in motion) while the monopole and receiver are moving in the negative x-direction. Note that the acoustic pressure field calculated for the latter case can be equivalent to the acoustic pressure field generated from the case of the static monopole and static receiver in the moving fluid medium.

First, consider the case of the moving monopole at a constant velocity, U in the negative x-direction while the receiver is not in motion in a static fluid medium.[14] Then, the non-homogeneous wave equation can be written as

$$\nabla^2 p-\frac{1}{c_0^2}\frac{\partial^2 p}{\partial t^2}=-q(t)\delta(x+Ut)\delta(y)\delta(z), \tag{B1}$$

where q is the monopole strength that represents the total rate of mass flux out of the source.[14] By applying the Lorenz Transform to Eq. (B1), the solution of Eq. (B1) can be represented as[14]

$$p(\mathbf{r},t)=\frac{q(t-R/c_0)}{4\pi R_1}, \tag{B2}$$

where

$$R=\frac{-M(x+Ut)+R_1}{1-M^2}, \tag{B3}$$

and

$$R_1=\sqrt{(x+Ut)^2+(1-M^2)(y^2+z^2)}. \tag{B4}$$

Note that in Eqs. (B2)–(B4), M is the Mach number defined as

$$M=\frac{U}{c_0}. \tag{B5}$$

When the receiver is moving at the constant velocity of U, the following coordinate transformation can be defined as

$$x=\chi-Ut, \tag{B6}$$

where χ is the receiver's x-coordinate. Define also $y=\psi$ and $z=\zeta$ where (ψ,ζ) are the receiver's (y,z) coordinates. By substituting Eq. (B6) into Eqs. (B2)–(B4), the acoustic pressure field radiated from a fixed monopole in the moving fluid medium can be found. Note that in the resulting expression of the sound field, R and R_1 are not the function of time, and no Doppler's effect is thus present: i.e., there is no frequency modulation due to the motion of the fluid medium. Therefore, the resulting sound field can be directly transformed to a frequency domain. The complex acoustic pressure field in the frequency domain is then represented as

$$p(\mathbf{r})=\frac{Q(\omega)\exp(ikR)}{R_1}, \tag{B7}$$

where

$$R=\frac{-M\chi+R_1}{1-M^2} \tag{B8}$$

and

$$R_1=\sqrt{\chi^2+(1-M^2)(\psi^2+\zeta^2)}. \tag{B9}$$

Note that in Eq. (B7), $Q(\omega)$ is the Fourier Transform of $q(t)$ and the harmonic exponential function, $\exp(-i\omega t)$ is omitted for the compact expression.

[1] J. D. Maynard, E. G. Williams, and Y. Lee, "Nearfield acoustic holography: I. Theory of generalized holography and the development of NAH," J. Acoust. Soc. Am. **78**, 1395–1413 (1985).
[2] W. A. Veronesi and J. D. Maynard, "Nearfield acoustic holography (NAH): II. Holographic reconstruction algorithms and computer implementation," J. Acoust. Soc. Am. **81**, 1307–1322 (1987).
[3] E. G. Williams, *Fourier Acoustics: Sound Radiation and Nearfield Acoustical Holography* (Academic, San Diego, CA, 1999), pp. 15–114.
[4] J. Hald, "Patch near-field acoustical holography using a new statistically optimal method," in Proceedings of Inter-Noise (2003), pp. 2203–2210.
[5] J. Hald, "Patch near-field acoustical holography using a new statistically optimal method," Brüel & Kjær Technical Review No. 1, Brüel & Kjær, pp. 40-50, 2005.
[6] Y. T. Cho, J. S. Bolton, and J. Hald, "Source visualization by using statistically optimized near-field acoustical holography in cylindrical coordinates," J. Acoust. Soc. Am. **118**, 2355–2364 (2005).
[7] E. G. Williams, "Continuation of acoustic near-fields," J. Acoust. Soc. Am. **113**, 1273–1281 (2003).

[8]M. Lee and J. S. Bolton, "Reconstruction of source distributions from acoustic pressures measured over discontinuous region: Multipatch holography and interpolation," J. Acoust. Soc. Am. **121**, 2086–2096 (2007).
[9]J. Hald, "STSF—A unique technique for scan-based nearfield acoustical holography without restriction on coherence," Brüel & Kjær Technical Review No. 1, Brüel & Kjær, pp. 1-50, 1989.
[10]H.-S. Kwon, Y.-J. Kim, and J. S. Bolton, "Compensation for source nonstationarity in multireference, scan-based near-field acoustical holography," J. Acoust. Soc. Am. **113**, 360–368 (2003).
[11]Y.-J. Kim, J. S. Bolton, and H.-S. Kwon, "Partial sound field decomposition in multireference near-field acoustical holography by using optimally located virtual references," J. Acoust. Soc. Am. **115**, 1641–1652 (2004).
[12]R. J. Ruhala and D. C. Swanson, "Planar near-field acoustical holography in a moving medium," J. Acoust. Soc. Am. **122**, 420–429 (2007).
[13]H.-S. Kwon, "Sound visualization by using enhanced planar acoustic holographic reconstruction," Ph.D. thesis, Korea Advanced Institute of Science and Technologies, South Korea (1997).
[14]P. M. Morse and K. U. Ingard, *Theoretical Acoustics* (Princeton University, Princeton, NJ, 1987), pp. 698–780.